American Mineralogist, Volume 78, pages 921–931, 1993

Mg-Fe order-disorder reaction in Fe-rich orthopyroxene: Structural variations and kinetics

Julia A. Sykes-Nord
43968 Tavern Drive, Ashburn, Virginia 22011, U.S.A.
Gian Mario Molin
CNR, Centro di Studio Problemi Orogeno Alpi Orientali, Dipartimento di Mineralogia e Petrologia, Università di Padova, Corso Garibaldi 37, I-35100 Padua, Italy

Abstract

Single-crystal X-ray techniques were used to study isothermal Fe^{2+}-Mg disordering in two orthopyroxene samples, Opx 4 (Fs_{61}) and Opx 5 (Fs_{85}), at temperatures of 625, 675, 725 °C and 525, 575, and 625 °C, respectively. Heating was continued until cation distributions reached steady state, which was considered equilibrium. The structure data obtained correlate very well with all other work on orthopyroxene, including natural (heated and unheated) crystals and synthetic end-members. These crystallographic variations also provide an internal constraint on the disordering process.

Instability of the orthopyroxene crystal structure was noted for some crystals where heating was continued after cation distribution equilibrium was attained. This was indicated by a decrease in Fe^{2+} in the M2 site, with no corresponding increase in Fe^{2+} in the M1 site. In addition, there was a small decrease in the size of the M1 site, which is thought to be caused by vacancy introduction in the M2 site, with Fe^{2+}-Fe^{3+} substitution in the M1 site and the Fe sublimating during heating.

The Mueller chemical rate law was used to calculate rate constants of 4.70×10^9 and (1.97×10^9)/min and activation energies of 47.1 and 41.3 kcal/mol for Opx 4 and Opx 5, respectively. From these results, together with values in the literature, we have shown that a distinct step is found at Fs_{50}–Fs_{60} in the activation energies, with higher activation energies of approximately 60 kcal/mol for Mg-rich samples and lower activation energies of approximately 50 kcal/mol for the Fe-rich samples. The rate constants of Opx 4 and Opx 5 are comparable with previously determined disordering rates.

Introduction

In orthopyroxenes with space group *Pbca,* long-range order-disorder occurs between divalent Mg and Fe^{2+} atoms in the two M sites, with Fe^{2+} preferring the larger M2 site (Ghose, 1961, and subsequent workers). The distribution of Mg and Fe^{2+} varies as a function of temperature (becoming more ordered at lower temperatures) and chemical composition. Studies of the equilibrium order are essential to the theoretical thermodynamic calculation of pyroxene solvi (Lindsley, 1983; Saxena, 1983a, 1983b; Davidson, 1985; Davidson and Lindsley, 1985) and a more complete understanding of the two-pyroxene geothermometer. Disequilibrium studies can be used to give activation energies and reaction rates of both ordering and disordering reactions and lead to a better understanding of the subsolidus processes occurring in orthopyroxene-bearing rocks.

Fe^{2+}-Mg order-disorder in natural and equilibrated orthopyroxenes has been investigated experimentally by Ghose (1965), Evans et al. (1967), Virgo and Hafner (1969, 1970), Saxena and Ghose (1971), Smyth (1973), Khristoforov et al. (1974), Besancon (1981), Domeneghetti et al. (1985), Sposato and Besancon (1987), Anovitz et al. (1988), Saxena et al. (1989), and Molin et al. (1991). Only Virgo and Hafner (1969), Anovitz et al. (1988), and Molin et al. (1991) reversed the experiments. Kinetics of the intracrystalline distribution in orthopyroxenes have been studied by Virgo and Hafner (1969), Besancon (1981), Anovitz et al. (1988), Saxena et al. (1989), and Molin et al. (1991). These kinetic studies were all conducted using the Mössbauer technique except those of Saxena et al. (1989) and Molin et al. (1991), where single-crystal X-ray diffraction was used. Much of this work has been reviewed previously (Ganguly, 1982; Anovitz et al., 1988). In addition, a comparison of site occupancy results from both Mössbauer and single-crystal X-ray diffraction has been made by Skogby et al. (1992) for five orthopyroxene crystals.

In our study, disordering experiments were undertaken to determine structural changes and equilibrium site occupancies (i.e., no further change with time) for heated and unheated Fe^{2+}-rich orthopyroxene crystals. Site occupancies were determined by single-crystal X-ray refinements of progressively heated crystals following intracrystalline exchange.

0003–004X/93/0910–0921$02.00

TABLE 1. Composition of Opx 4 and Opx 5

	Opx 4	Opx 5	Opx 5*
SiO_2	50.3	47.9	46.53
TiO_2	0.1	0.0	0.05
Al_2O_3	0.0	0.4	0.76
Cr_2O_3	0.1	0.0	0.01
FeO**	34.6	47.4	45.58
Fe_2O_3	0.0	0.0	2.80
MnO	0.6	0.2	0.36
MgO	12.3	4.5	4.60
CaO	1.2	1.2	1.13
Na_2O	0.0	0.0	0.02
Total	99.2	101.6	101.84
Molecular proportions per six O atoms			
Si	2.01	1.99	1.94
Ti	0.00	0.00	0.00
Al	0.00	0.02	0.04
Cr	0.01	0.00	0.00
Fe^{2+}	1.16	1.65	1.59
Fe^{3+}	0.00	0.00	0.09
Mn	0.02	0.01	0.01
Mg	0.73	0.28	0.29
Ca	0.05	0.05	0.05
Na	0.00	0.00	0.00
Total	3.98	4.00	4.01

Note: compositions are in weight percent.
* Wavelength-dispersive analysis.
** Fe^{3+}/Fe^{2+} calculated by MINCLC (Freeborn et al., 1985).

The ensuing work can be divided into two main sections. The first section focuses on crystallographic variations of the orthopyroxene structure on heating. This provides an inherent constraint on the disordering process lacking in the previous Mössbauer studies. In addition, the crystallographic parameters indicate problems in the stability of Fe-rich orthopyroxene on heating at the experimental pressure of 1 bar. Therefore, ordering experiments that necessitate initial heating at a high temperature were not attempted. In the second section, reaction rates for the disordering reaction are calculated from the chemical rate law, as developed by Mueller (1962, 1967, 1969). These are compared with previous work on both disordering and ordering and discussed with respect to composition and temperature. From these results, activation energies are calculated. The problems of using a chemical rate law are discussed and a possible alternative approach suggested.

Experimental and refinement techniques

Samples

Two Fe^{2+}-rich orthopyroxenes (Opx) have been chosen for this study, both from granulite facies metamorphic rocks. Opx 4 [$Fe^{2+}/(Fe^{2+} + Mg) = 0.61$] is from Uusima, Finland (Saxena, 1969); Opx 5 [$Fe^{2+}/(Fe^{2+} + Mg) = 0.85$] is from a metamorphosed Fe formation in the Wind River Mountains in Wyoming (Sykes, 1984). The compositional data are given in Table 1.

Procedures

The following procedure was applied to every crystal: (1) X-ray data measurement and structure refinement of the unheated crystal were obtained. (2) Isothermal heating experiments in silica tubes were conducted on the same crystal until a close approximation of the exchange equilibrium was reached. The experiments were conducted at three temperatures for each composition: 525, 575, 625 °C for Opx 5; 625, 675, 725 °C for Opx 4. Remounting of the crystal, X-ray data measurement, and structure refinements were carried out after every heating. (3) X-ray energy-dispersive analysis of the same crystal was performed after the last X-ray data measurements.

Sample preparation and analysis

Clear, inclusion-free, equidimensional crystals of orthopyroxene (100–200 μm) with no visible exsolution lamellae and perfect extinction parallel to **c** were used.

An energy-dispersive spectrometer, EDS EG&G, connected to a SEM Autoscan electron microscope operating at 15 keV was employed to analyze the single crystals (Table 1). A Magic program (Colby, 1972) in the Ortec Magic IV M. version was used to convert X-ray counts into oxide weight percent. The analyses were averaged over several spots. In addition, Opx 5 was analyzed at the U.S. Geological Survey using an ARL-SEMQ microprobe and the Bence-Albee data reduction method. These results are also noted in Table 1. The microprobe data agree with the X-ray energy-dispersive analysis, except that the WDA analysis gives 2.8% Fe_2O_3 after recalculation by the program MINCLC (Freeborn et al., 1985).

Heating experiments

The crystals were sealed in small silica tubes containing pure Ar (fluxed at 800 °C with Ti and passed over anhydrous silica gel) at slightly above 1 atm. The durations of the heating experiments were initially chosen by consideration of the temperature, the composition of the pyroxene, and the results of previous work (Saxena and Ghose, 1971; Besancon, 1981). The sample was heated in a vertical, temperature-controlled furnace [± 3 °C, Pt/(Pt-Rh) thermocouple]. Quenching of the crystal was done by dropping the tube into cold H_2O.

X-ray data measurement and structural refinement

Intensity data were obtained by using a computer-controlled Siemens AED four-circle diffractometer with Mo$K\alpha$ radiation monochromatized by a flat graphite crystal at Padua, Italy. Intensities of reflections with $\theta \leq 30°$ were measured using the ω-scan mode. The equivalent pairs hkl and $\bar{h}kl$ were scanned. The intensities were corrected for absorption following the semiempirical method of North et al. (1968), and the values of the equivalent pairs were averaged. The X-ray data were processed by means of a program specifically written for the STOE AED II diffractometer; one of its standard programs (DL) was used to optimize the unit-cell parameters.

The refinements were carried out in space group *Pbca* without chemical constraints using a full-matrix least-squares program (BLSQ cop. STOE). (The site partition-

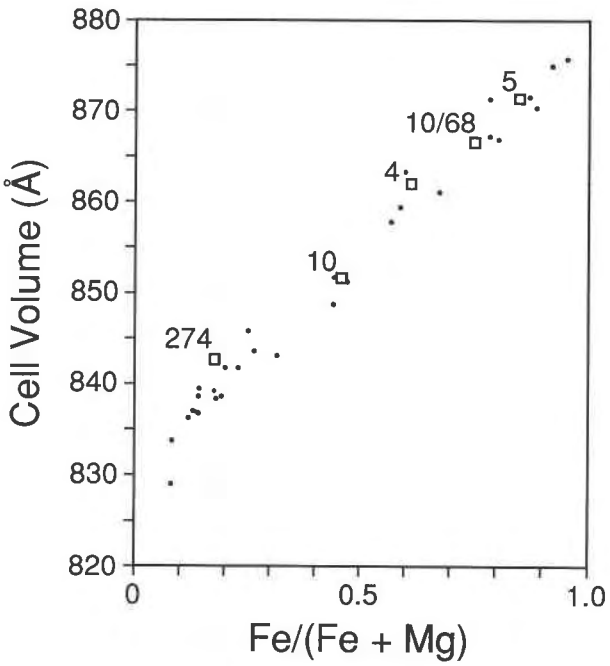

Fig. 1. Variation of the unit-cell volume with composition. Solid circles are for samples from Ross and Huebner (1979). Samples 4 and 5 are from this study, and samples 274, 10, and 10/68 are from Domeneghetti et al. (1985).

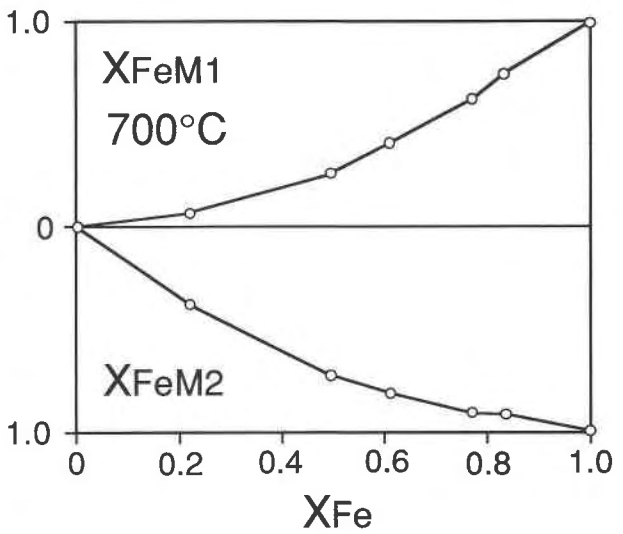

Fig. 2. Filling of both the M1 and M2 sites in orthopyroxene with respect to total Fe^{2+} content at 700 °C. Samples indicated are the same as in Fig. 1.

ing used to obtain the reaction rates is calculated using both structure site occupancies and the chemical composition of the sample, as discussed later.) This refinement program allows assignment of two scattering curves (f1 and f2) for each site and refinement of the occupancy factors x(f) with the constraint that x(f1) + x(f2) = 1. Since the maximum difference between neutral and ionized scattering curves occurs at low $\sin(\theta/\lambda)$ values (up to 0.30), a partial ionization model was adopted (Rossi et al., 1983). Fully ionized cations were assigned to the M1 and M2 sites (Mg^{2+} and Fe^{2+} for M1; Mg^{2+} and Fe^{2+} for M2), a partly ionized Si cation ($Si^{2.5+}$) for TA and TB, and a negative charge ($O^{1.5-}$) for the O sites (Comer and Waber, 1974; Tokonami, 1965). All of the structure sites were considered fully occupied. The reflections with $I \geq 3\sigma(I)$ were considered as observed and were given equal weight. All of the displacement factors were treated as isotropic at first and then as anisotropic, starting with the atomic and thermal parameters of Ganguly and Ghose (1979).

Selection of crystals of suitable quality was difficult. Approximately one crystal in six for Opx 4 (R discrepancy values 2.7–3.9%) and one crystal in four for Opx 5 (R discrepancy values 2.9–3.9%) were selected for the heating experiments after initial study by X-ray diffraction. R values of 2.7–4.4% were obtained for the heated crystals. The resulting standard errors in site occupancies are 0.006–0.009 apfu. Final atomic parameters and observed and calculated structure factors are available from the authors. Structure data utilized in this paper are given in Table 2.

Effects of heating on the structure of orthopyroxene

Crystallographic variations

The structure data for both the heated and unheated crystals of this study are consistent with previous data on orthopyroxenes (Domeneghetti et al., 1985, samples 274,10,10/68) and the synthetic end-members enstatite (Ganguly and Ghose, 1979) and ferrosilite (Sueno et al., 1976). Structure data are compiled in Table 2. The values X_{FeM1} and X_{FeM2} are the crystallographic site occupancies calculated from electron density at the sites, assuming that only Fe^{2+} and Mg are present.

Variations in the volume of the unit cell are essentially linear with respect to the Fe/(Fe + Mg) content (Fig. 1). Data for the samples are compared with those of unheated samples of both Ross and Huebner (1979) and Domeneghetti et al. (1985). With heating, the unit-cell volume increases because Fe^{2+} enters and enlarges the smaller M1 site, as shown by the slight increase in M1-O. The volume change on heating, although noted (Table 2) for each individual crystal, is within the symbol size on Figure 1.

The distribution of Fe^{2+} between the two M sites is not equal, in agreement with previous studies. We have clearly shown this distribution in Figure 2. With increasing X_{Fe}, Fe^{2+} first enters the M2 site. Then, when X_{Fe} is between 0.5 and 0.6 and the M2 site is almost saturated with Fe^{2+}, the additional Fe^{2+} fills the M1 site preferentially. Other physical changes occurring at this compositional range are a break in the slope of the tie line rotation between orthopyroxene and clinopyroxene (Ross and Huebner, 1975) and a change in the activation energy of

Table 2. Structural data for Opx 4 from Finland and Opx 5 from Wyoming

T (°C)	t (min)	X_{FeM1}	X_{FeM2}	M1 + M2 electron no.*	Cell V (Å^3)	TA-O mean (Å)	TA-O bridging (Å)	TA-O nonbridging (Å)	TB-O mean (Å)	TB-O bridging (Å)	TB-O nonbridging (Å)
					Opx 4						
25	unh	0.300	0.939	41.346	861.940	1.626	1.645	1.606	1.639	1.667	1.610
625	20	0.352	0.892	41.416	862.520	1.626	1.647	1.605	1.641	1.667	1.614
625	40	0.370	0.859	41.206	862.870	1.628	1.648	1.610	1.640	1.670	1.610
625	60	0.391	0.850	41.374	862.850	1.626	1.647	1.605	1.638	1.668	1.608
625	120	0.393	0.834	41.178	862.560	1.626	1.647	1.605	1.641	1.669	1.613
625	300	0.403	0.824	41.178	862.720	1.627	1.647	1.606	1.640	1.668	1.612
625**	1800	0.408	0.802	40.940	862.660	1.628	1.647	1.609	1.639	1.666	1.612
625**	6000	0.411	0.746	40.198	860.750	1.625	1.643	1.606	1.637	1.664	1.610
25	unh	0.296	0.953	41.486	861.560	1.625	1.646	1.605	1.638	1.667	1.610
25†	unh	0.291	0.937	41.192	862.420	1.626	1.647	1.605	1.640	1.669	1.611
675†	10	0.352	0.879	41.234	863.070	1.626	1.648	1.604	1.640	1.671	1.610
675	15	0.362	0.860	41.108	863.270	1.627	1.647	1.608	1.639	1.668	1.610
675	30	0.387	0.841	41.192	863.400	1.628	1.646	1.609	1.640	1.670	1.609
675†	30	0.378	0.844	41.108	863.440	1.627	1.649	1.606	1.640	1.669	1.619
675	45	0.392	0.839	41.234	863.820	1.626	1.648	1.603	1.640	1.669	1.611
675†	120	0.392	0.832	41.136	863.980	1.626	1.648	1.603	1.641	1.671	1.611
25	unh	0.288	0.942	41.220	861.603	1.625	1.644	1.607	1.638	1.667	1.609
725	5	0.425	0.804	41.206	862.780	1.624	1.645	1.602	1.639	1.669	1.608
725	10	0.411	0.789	40.800	862.520	1.625	1.645	1.604	1.640	1.668	1.612
725	15	0.422	0.784	40.884	862.280	1.626	1.649	1.603	1.641	1.667	1.614
725	45	0.422	0.784	40.884	862.420	1.626	1.646	1.607	1.635	1.667	1.603
725**	180	0.426	0.740	40.324	860.870	1.625	1.647	1.604	1.638	1.665	1.610
					Opx 5						
25	unh	0.713	0.959	47.408	871.440	1.626	1.645	1.607	1.641	1.669	1.614
525	5	0.720	0.965	47.590	871.650	1.626	1.644	1.609	1.642	1.666	1.618
525	15	0.719	0.950	47.366	871.550	1.623	1.644	1.602	1.639	1.666	1.613
525	30	0.731	0.962	47.702	871.420	1.627	1.647	1.607	1.641	1.668	1.614
525	120	0.747	0.945	47.688	871.520	1.625	1.644	1.606	1.642	1.668	1.616
525**	34560	0.741	0.893	46.876	871.050	1.627	1.644	1.609	1.641	1.666	1.615
25	unh	0.704	0.958	47.268	871.640	1.626	1.645	1.607	1.641	1.667	1.615
575†	5	0.717	0.948	47.310	871.940	1.626	1.645	1.608	1.643	1.668	1.618
575†	10	0.690	0.925	46.610	871.610	1.626	1.646	1.606	1.639	1.666	1.613
575	15	0.718	0.935	47.142	871.840	1.627	1.647	1.607	1.645	1.668	1.617
575	30	0.713	0.929	46.988	871.950	1.625	1.646	1.605	1.642	1.670	1.614
575†	120	0.718	0.933	47.114	872.150	1.627	1.647	1.607	1.642	1.669	1.614
575†	600	0.726	0.928	47.156	872.550	1.628	1.649	1.606	1.644	1.669	1.619
25	unh	0.708	0.956	47.296	871.970	1.626	1.644	1.608	1.642	1.667	1.617
25†	unh	0.714	0.963	47.478	872.010	1.626	1.644	1.608	1.640	1.668	1.613
625†	5	0.740	0.917	47.198	872.150	1.624	1.643	1.606	1.643	1.668	1.617
625	10	0.732	0.920	47.128	871.990	1.626	1.644	1.608	1.641	1.670	1.612
625	20	0.740	0.920	47.240	872.600	1.627	1.645	1.610	1.639	1.670	1.608
625	30	0.744	0.918	47.268	872.131	1.625	1.645	1.605	1.641	1.668	1.613
625	90	0.747	0.913	47.240	871.720	1.626	1.646	1.607	1.640	1.666	1.615
625	270	0.749	0.918	47.338	871.700	1.625	1.644	1.607	1.640	1.666	1.613

Note: the abbreviation unh = unheated.
* See text for calculation.
** Problem with stability.
† Second crystal studied.

disordering, as we have noted. These observations are discussed later.

The tetrahedral sites TA and TB show slight geometrical variations (Table 2). The general trend with increasing $X_{FeM1} + X_{FeM2}$ content is for a lengthening of the ⟨T-O⟩ nonbridging distances and a shortening of the ⟨T-O⟩ bridging bond distances. The mean ⟨T-O⟩ distances for both A and B chains do not change significantly with increasing $X_{FeM1} + X_{FeM2}$. Data for Opx 5 support the observation (Domeneghetti et al., 1985) that $^{[4]}$Al substitution occurs only in the TB site, resulting in an increase in the ⟨TB-O⟩ bond lengths, especially for the ⟨TB-O⟩ nonbridging bonds.

The M2 site has an irregular coordination with six O atoms. Figure 3a shows the variation in the M2-O3A bond length with respect to $X_{FeM1} + X_{FeM2}$ for the unheated samples. The regular increase in the M2-O3B bond length with composition is shown in Figure 3b. As discussed by Domeneghetti et al. (1985), this regular increase in the bond lengths between the M2 site and the bridging O3 atoms with $X_{FeM1} + X_{FeM2}$ indicate that these bonds are sensitive to the bulk octahedral layer size rather than the single M2 site. Samples 10 and 5 have slightly shorter M2-O3B bond lengths. This observation complements the increase in size of the ⟨TB-O⟩ bond lengths caused by a small amount of $^{[4]}$Al in the TB site, as suggested by Domeneghetti et al. (1985).

The M1 octahedral site shows a wide variation in size

TABLE 2—*Continued*

M1-O mean (Å)	M2-O mean (Å)	M2-O3A (Å)	M2-O3B (Å)	M2 *V* (Å³)	M1 *V* (Å³)
			Opx 4		
2.103	2.222	2.414	2.560	13.413	12.26
2.103	2.219	2.408	2.556	13.378	12.266
2.105	2.217	2.405	2.553	13.364	12.291
2.105	2.220	2.406	2.554	13.404	12.30
2.104	2.217	2.407	2.551	13.36	12.104
2.105	2.218	2.406	2.557	13.35	12.29
2.103	2.219	2.407	2.561	13.38	12.27
2.101	2.221	2.408	2.565	13.42	12.23
2.102	2.221	2.414	2.561	13.40	12.241
2.103	2.221	2.415	2.558	13.403	12.255
2.106	2.219	2.412	2.554	13.366	12.314
2.105	2.219	2.411	2.557	13.39	12.290
2.106	2.218	2.410	2.556	13.36	12.32
2.105	2.218	2.404	2.556	13.37	12.29
2.108	2.218	2.409	2.555	13.36	12.348
2.108	2.218	2.410	2.554	13.358	12.351
2.101	2.222	2.416	2.555	13.429	12.240
2.106	2.217	2.406	2.553	13.35	12.32
2.106	2.216	2.407	2.552	13.331	12.306
2.105	2.217	2.404	2.556	13.343	12.295
2.105	2.221	2.406	2.562	13.42	12.302
2.102	2.219	2.404	2.551	13.40	12.25
			Opx 5		
2.119	2.224	2.441	2.563	13.442	12.545
2.120	2.223	2.445	2.567	13.426	12.55
2.120	2.227	2.446	2.569	13.506	12.588
2.120	2.220	2.438	2.563	13.42	12.553
2.120	2.223	2.441	2.563	13.42	12.56
2.117	2.227	2.440	2.572	13.49	12.51
2.119	2.227	2.445	2.566	13.50	12.55
2.118	2.226	2.441	2.563	13.48	12.515
2.120	2.228	2.442	2.572	13.52	12.56
2.119	2.225	2.438	2.563	13.44	12.54
2.121	2.223	2.441	2.561	13.43	12.58
2.121	2.224	2.438	2.563	13.46	12.57
2.119	2.225	2.439	2.563	13.45	12.54
2.118	2.226	2.444	2.562	13.46	12.52
2.118	2.228	2.444	2.570	13.514	12.53
2.120	2.225	2.446	2.568	13.457	12.56
2.121	2.226	2.443	2.562	13.49	12.56
2.122	2.227	2.443	2.567	13.505	12.591
2.122	2.226	2.441	2.568	13.482	12.583
2.119	2.229	2.444	2.574	13.527	12.53
2.119		2.442	2.574		

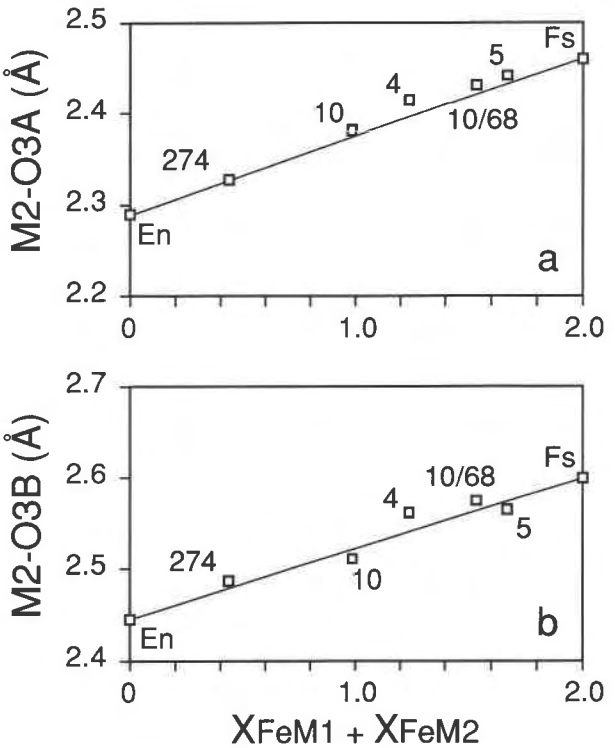

Fig. 3. Variation in (**a**) M2-O3A and (**b**) M2-O3B bond lengths with $X_{FeM1} + X_{FeM2}$ for the unheated samples. Samples are the same as in Fig. 1, with the additional samples En from Ganguly and Ghose (1979) and Fs from Sueno et al. (1976). Estimated errors of ±0.003 Å are within the size of the symbol.

with heating. In Figure 4, the variation in the mean ⟨M1-O⟩ bond length with respect to time is shown. The change in bond lengths is more pronounced for Opx 4 than Opx 5, as there is a much greater possibility for disorder due to the larger amount of Mg. Initially, the ⟨M1-O⟩ bond length increases as expected with increasing Fe^{2+} entering the M1 site. However, with further heating the ⟨M1-O⟩ bond length decreases significantly, with almost constant X_{FeM1}. This effect, not related to the degree of disorder, will be discussed below.

Stability of Fe^{2+}-rich orthopyroxene

Both Opx 4 and 5 showed signs of structural instability with heating of the crystals. After every cycle of refinement, an estimate of the total number of electrons in the M1 and M2 sites was calculated from the refined occupancy factors, assuming 26 and 12 electrons for Fe and Mg, respectively (Table 2). The M1 + M2 electron number should remain approximately constant throughout the experiment. For three crystals, Opx 4 at 625 and 725 °C and Opx 5 at 525 °C, there was a marked decrease in the number of electrons after several periods of heating (Fig. 4a–4c). This coincided with a decrease in the amount of Fe^{2+} in the M2 site, with no corresponding increase in Fe^{2+} in the M1 site, indicating that this effect is not related to the order-disorder reaction. In addition, there was a small decrease in the M1-O distances for the M1 site. (It should also be noted that Anovitz et al., 1988, reported anomalous results for their most Fe^{2+}-rich sample [PX4, TM2, Fe/(Fe + Mg) = 0.81] for long periods of heating.)

This decrease in the calculated number of electrons with time could be attributed to a loss of Fe^{2+} (or other high electron density ions) from the orthopyroxene crystal structure, essentially from the M2 site. There are several possible explanations for this observation including (1) oxidation of the sample with formation of Fe^{3+} oxides, (2) formation of a secondary Fe^{2+}-rich phase within the crystal, or (3) the introduction of vacancies.

Fe^{2+}-rich orthopyroxenes are only stable at relatively

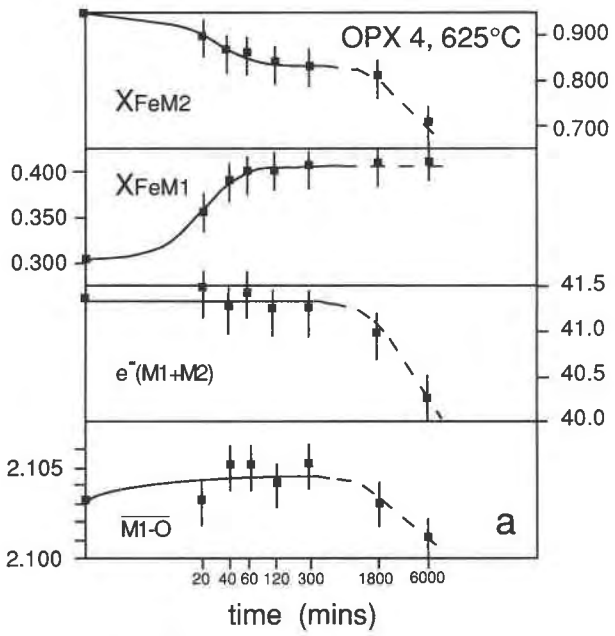

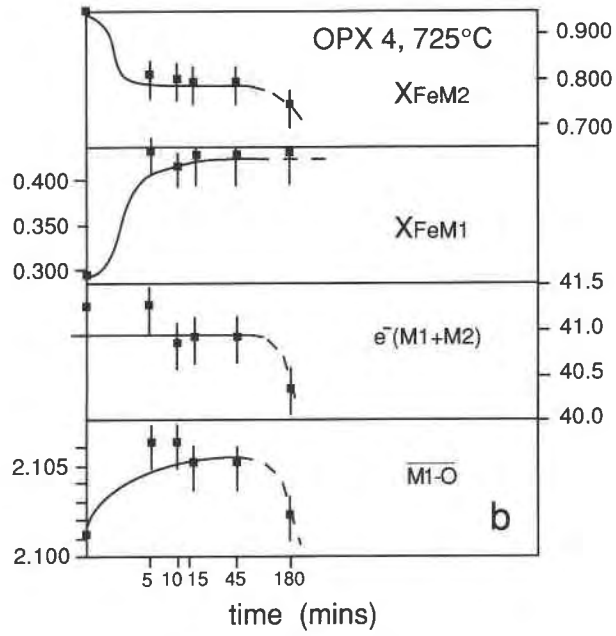

Fig. 4. (a–c) Summary of three of the heating experiments showing crystal instability. The dashed line indicates trends outside the stability conditions.

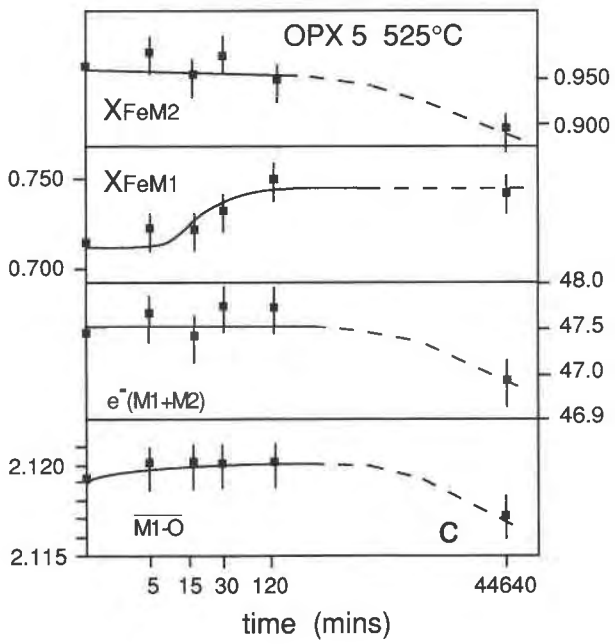

high temperatures and pressures, normally associated with granulite facies metamorphism. The equilibrium conditions for orthopyroxene, relative to olivine and quartz, are dependent not only on pressure and temperature but also on f_{O_2}. The actual value of f_{O_2} attained during annealing of Opx 4 and Opx 5 is not known. In order to evaluate any changes that would indicate oxidation or reduction, we have examined crystals of heated and unheated Opx 4 and Opx 5 by transmission and scanning electron microscopy.

A first approximation to the relative stabilities of orthopyroxenes having the compositions of the studied samples can be obtained from the phase diagram of Chatterjee (1987) (Fig. 5). The f_{O_2} appropriate for this phase diagram is below the QFM buffer. The phase diagram is contoured for the composition of the Fe^{2+}-rich pyroxene. P-T conditions for Opx 5 exceed the limits of the stability field at 1 atm at all temperatures considered. However, Opx 4, if a pure quadrilateral phase, should be stable up to approximately 950 °C. Small amounts of nonquadrilateral components may cause it to become unstable at lower temperatures. The Fe-rich sample of Anovitz et al. (1988) also plots out of the orthopyroxene stability field at the temperatures and pressures of their experiments. Anovitz et al. (1988) obtained X-ray diffraction patterns of the anomalous samples, but no other phases were detected.

Heated and unheated samples of Opx 5 (700 °C, 15 h) were studied by SEM and TEM. No surface phases were seen on either crystal in SEM images; X-ray energy-dispersive analyses of parts of the crystal surface gave no indication of an oxide phase. Therefore, oxidation due to introduction of O seems unlikely. In both samples small lamellae (<2% by area) of $C2/c$ clinopyroxene were observed in TEM images, as expected for granulite facies pyroxenes. If these lamellae were homogenized during the heating experiment, Ca^{2+} that entered the M2 site may have had an unknown effect on the disordering reaction. However, other rate studies on clinopyroxenes of similar Fe/Mg ratios indicate that significantly higher temperatures and long times are necessary for any long-range diffusion (tens of nanometers) that might affect the rate law (Nord and McCallister, 1979; Buseck et al., 1980).

No indication of any other secondary phase could be seen in TEM images, and no structure distortions were noted.

With the data available from these experiments, the exact nature of the electron loss cannot be determined; however, it appears that the introduction of vacancies in the M2 site (i.e., the removal of Fe^{2+}) is the most likely cause. The decrease in the M1-O mean bond length occurring while the amount of Fe in the site remains constant suggests a substitution of Fe^{3+} for Fe^{2+} in M1, which would maintain the charge balance of the crystal. It is inferred that a small amount of Fe sublimated during heating. It is important to be aware of these problems both for future experimentation and when using previously published data in the compositional range Fs_{60}–Fs_{95}.

Reaction rates and activation energies

Calculation of cation distribution

The structure data obtained in this study, together with the microprobe data, have been used to calculate cation distributions to analyze the kinetics of the disordering exchange reaction in orthopyroxene, dominated by

$$Mg^{2+}\ M1 + Fe^{2+}\ M2 \rightarrow Fe^{2+}\ M1 + Mg^{2+}\ M2. \quad (1)$$

Other components in the crystal (Ca^{2+}, Mn^{2+}, Cr^{3+}, Ti^{4+}, Al^{3+}) will also affect the exchange reaction. The cation distributions used for the calculations of reaction rates in this paper have been calculated from the X-ray site occupancies using the program MINUIT (James and Roos, 1975). Ca^{2+} and Mn^{2+} were assigned to the M2 site and $^{[6]}Al$, Fe^{3+}, Cr^{3+}, and Ti^{4+} to the M1 site (Tazzoli and Domeneghetti, 1987; Molin, 1989). Mg^{2+} and Fe^{2+} distributions are obtained by the minimization of the squares of the normalized residuals of the following constraints (after Cundari and Salviulo, 1987): (1) the balance between atomic fractions and site electron densities of M1 and M2, (2) the sites TA, TB, M1, and M2 are completely occupied, (3) charge balance between $^{[4]}Al$ and R^{3+}, (4) bulk valence balance (converts Fe^{2+} to Fe^{3+}). The site occupancies are reported in Table 3.

The results of this study are compared with those of previous studies (Besancon, 1981; Anovitz et al., 1988), where the relative proportions of Fe^{2+} and Fe^{3+} in the two M sites were determined by Mössbauer methods, and cation distributions were calculated from Fe_{tot} of the sample, as determined by chemical analysis. The terms X_{FeM1} and X_{FeM2} were introduced above as the calculated Fe and Mg distributions with the assumption that only Fe and Mg were present in the M sites. These values were useful for the comparison of crystal structure geometry with site occupancy and composition. For the reaction analysis, however, the actual site occupancies as reported in Table 3 must be used to compare the results with those of the Mössbauer analysis.

Reaction rate calculation

As in all previous studies of the order-disorder reaction in orthopyroxene, we have used the Mueller chemical rate law model (based on Dienes, 1955) to calculate the reaction rates. Using the Mueller model one can derive the following equation for the disordering reaction in pyroxenes where $\vec{k}$ is the rate constant for disordering:

$$\frac{-dX^{Fe}_{M2}}{dt} = \vec{k}[a(X^{Fe}_{M2})^2 + b(X^{Fe}_{M2}) + c]. \quad (2)$$

The parameters for orthopyroxene are defined as $a = \frac{1}{2}(1 - K_d^{-1})$, $b = \frac{1}{2} - X_{Fe} + K_d^{-1}(X_{Fe} + \frac{1}{2})$, and $c = -K_d^{-1}X_{Fe}$, and K_d is the distribution coefficient.

$$K_d = \frac{X^{Fe}_{M1}X^{Mg}_{M2}}{X^{Fe}_{M2}X^{Mg}_{M1}}$$

$$X_{Fe} = \tfrac{1}{2}(X^{Fe}_{M2}X^{Fe}_{M1})$$

where X^{Fe}_{M2} is the site mole fraction of Fe^{2+} in the M2 site.

Mueller integrated Equation 2, yielding

$$-\vec{k}\Delta t = \frac{1}{(b^2 - 4ac)^{1/2}} \cdot \ln\left|\frac{-(2aX^{Fe}_{M2} + b) + (b^2 - 4ac)^{1/2}}{(2aX^{Fe}_{M2} + b) + (b^2 - 4ac)^{1/2}}\right|_{X^{Fe}_{M2}(t0)}^{X^{Fe}_{M2}(t1)}.$$

The disordering rates calculated and their fit to the experimental data in this study are shown as a function of time in Figure 6. The reaction rates derived can be compared with previous studies of the Fe^{2+}-Mg exchange reaction in orthopyroxene. Besancon (1981) studied two

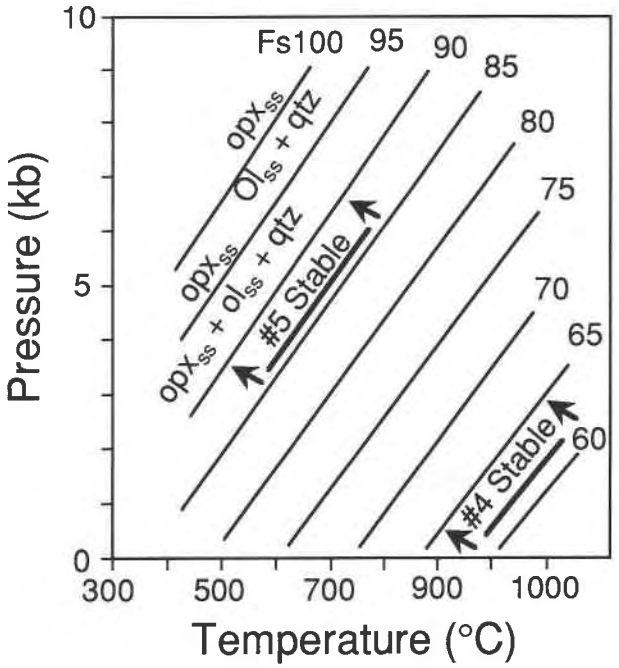

Fig. 5. Pressure-temperature phase equilibria for olivine, orthopyroxene, and quartz, contoured in mole percent ferrosilite (Fs) component. Thermochemical data used and f_{O_2} are given in the text.

TABLE 3. Site occupancies

T (°C)	t (min)	M1					M2			
		Mg^{3+}	Fe^{2+}	Fe^{3+}	Cr^{3+}	Ti^{4+}	Mg^{2+}	Fe^{2+}	Mn^{2+}	Ca^{2+}
					Opx 4					
25	unh	0.700	0.293	0.000	0.004	0.003	0.037	0.888	0.020	0.055
625	20	0.649	0.343	0.002	0.004	0.003	0.088	0.837	0.020	0.055
625	40	0.614	0.379	0.000	0.004	0.003	0.123	0.802	0.020	0.055
625	60	0.609	0.383	0.001	0.004	0.003	0.128	0.797	0.020	0.055
625	120	0.603	0.390	0.000	0.004	0.003	0.135	0.789	0.020	0.055
25	unh	0.702	0.289	0.002	0.004	0.003	0.023	0.904	0.020	0.053
675	10	0.646	0.345	0.002	0.004	0.003	0.097	0.830	0.020	0.053
675	15	0.636	0.355	0.002	0.004	0.003	0.116	0.811	0.020	0.053
675	30	0.611	0.380	0.002	0.004	0.003	0.135	0.792	0.020	0.053
675	45	0.606	0.385	0.002	0.004	0.003	0.155	0.772	0.020	0.053
25	unh	0.710	0.282	0.002	0.003	0.003	0.033	0.894	0.021	0.051
725	5	0.571	0.418	0.002	0.003	0.003	0.172	0.755	0.021	0.051
725	10	0.576	0.415	0.001	0.003	0.003	0.169	0.759	0.021	0.051
725	15	0.567	0.424	0.002	0.003	0.003	0.178	0.750	0.021	0.051
725	45	0.567	0.424	0.002	0.003	0.003	0.178	0.750	0.021	0.051

T (°C)	t (min)	M1				M2			
		Mg^{2+}	Fe^{2+}	Fe^{3+}	Al^{3+}	Mg^{2+}	Fe^{2+}	Mn^{2+}	Ca^{2+}
				Opx 5					
25	unh	0.272	0.717	0.003	0.008	0.006	0.933	0.007	0.054
525	5	0.271	0.718	0.004	0.007	0.007	0.932	0.007	0.054
525	15	0.265	0.722	0.006	0.006	0.013	0.926	0.007	0.054
525	30	0.262	0.729	0.000	0.009	0.016	0.923	0.007	0.054
525	120	0.246	0.744	0.003	0.008	0.032	0.907	0.007	0.054
25	unh	0.288	0.699	0.005	0.008	0.018	0.921	0.007	0.054
575	5	0.275	0.712	0.005	0.008	0.028	0.911	0.007	0.054
575	15	0.275	0.712	0.005	0.008	0.041	0.898	0.007	0.054
575	30	0.280	0.707	0.005	0.008	0.047	0.892	0.007	0.054
575	120	0.275	0.712	0.005	0.008	0.043	0.896	0.007	0.054
575	600	0.267	0.720	0.005	0.008	0.048	0.891	0.007	0.054
25	unh	0.274	0.716	0.002	0.008	0.004	0.935	0.007	0.054
625	10	0.243	0.747	0.001	0.009	0.035	0.904	0.007	0.054
625	20	0.240	0.748	0.006	0.006	0.038	0.900	0.007	0.054
625	30	0.235	0.756	0.000	0.009	0.043	0.896	0.007	0.054
625	90	0.231	0.759	0.001	0.009	0.047	0.892	0.007	0.054
625	270	0.235	0.751	0.010	0.004	0.044	0.895	0.007	0.054

Note: cation distributions calculated using the program MINUIT (James and Roos, 1975). The abbreviation unh = unheated.

TABLE 4. Summary of rate constants for disordering ($\vec{k}$), ordering ($\overleftarrow{k}$), and other kinetic data

Sample	HC*	274**	M32B†	10**	TZ*	4‡	10/68**	PX4§	5‡
Fe/(Fe + Mg)	0.13	0.18	0.39	0.49	0.61	0.57	0.77	0.81	0.85
T (°C)	$\vec{k}$	$\vec{k}$	$\overleftarrow{k}$	$\vec{k}$	$\vec{k}$	$\vec{k}$	$\vec{k}$	$\overleftarrow{k}$	$\vec{k}$
500			0.0000738					0.0003	
525									0.0095
550							0.0026		
575									0.048
600		0.0001	0.00732	0.003	0.000741		0.012	0.010	
625						0.0205			0.17
650‖	0.000454	0.000725	0.0523	0.0129	0.00448	0.0332	0.0467	0.045	0.333
675						0.0370			
700	0.00281	0.005	0.284	0.047	0.0147			0.15	
725						0.3			
750	0.0118				0.177				
800	0.0566	0.06	5.54		0.406			1.44	
k'/min	2.46×10^{11}	1.05×10^{11}	1.99×10^{13}	1.25×10^{9}	1.06×10^{12}	4.70×10^{9}	1.04×10^{9}	3.35×10^{13}	1.97×10^{9}
E (kcal/mol)	62.2	59.8	61.6	46.4	60.7	47.1	43.7	45.9	41.3

* From Table 3, Besancon (1981).
** Calculated from full site occupancy data of Saxena et al. (1989).
† Calculated from Eq. 26 of Anovitz et al. (1988).
‡ This study.
§ Calculated from Mössbauer analyses, Table 3 of Anovitz et al. (1988) because their Eq. 27 appears to be in error.
‖ Rates calculated from E and k' values.

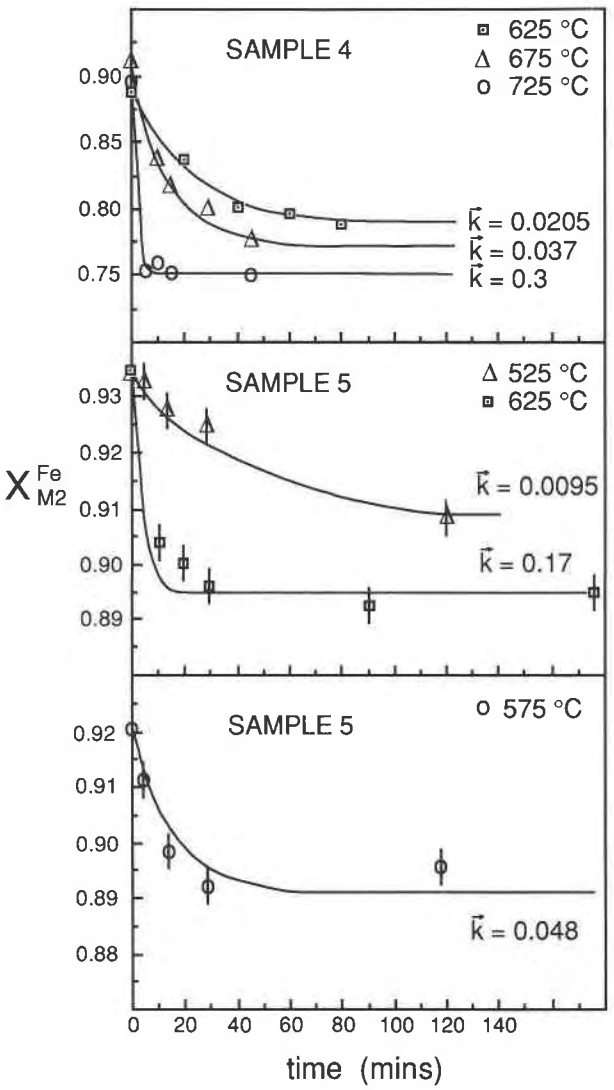

Fig. 6. Rate constant fits for samples 4 and 5 using the cation distributions from Table 3.

samples (HC, Fs_{13}, and TZ, Fs_{49}) using Mössbauer techniques, and Saxena et al. (1989) studied three samples (274, Fs_{18}; 10, Fs_{49}; and 10/68, Fs_{77}) using single-crystal X-ray techniques. Also included for comparison are the results of Anovitz et al. (1988). Two samples were studied (M32b, Fs_{39}, and PX4, Fs_{81}).

Table 4 shows the rate constants arranged by temperature and composition for all studies. As expected, the general trends are for the rates to increase with both increasing temperature and increasing Fe^{2+} content. These rate constants (disordering $\vec{k}$ and ordering $\overleftarrow{k}$) are also shown on Figure 7 (all recalculated to 650 °C). If the same process operates for all samples, a linear trend is expected for a plot of reaction rate vs. composition. The solid line shows the least-squares fit to the data, except for M32B. The rate constant, as calculated from the Mueller model, for sample M32B is one order of magnitude greater than

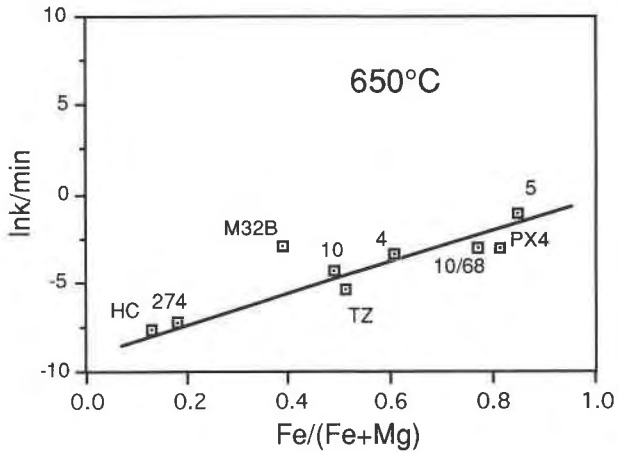

Fig. 7. Natural log of rate constants from Table 4 for both ordering and disordering at 650 °C with respect to composition.

for the other samples, whereas for sample PX4 (see note, Table 4) the ordering rate is equivalent to that expected for the disordering rate.

Activation energies

The data for rate constants can be used to obtain the activation energies and frequency factors for the order-disorder reaction. The rate constant

$$\vec{k} = k' \exp\left(\frac{-E_a}{RT}\right)$$

where k' = frequency or preexponential factor. This equation can be rewritten as

$$\ln \vec{k} = \frac{-E_a}{R}\left(\frac{1}{T}\right) + \ln k'.$$

The results can then be plotted on an Arrhenius diagram, and a straight line relationship is expected if the same mechanism is operable for each determination of $\vec{k}$. The slope of the line gives the activation energy of the process (divided by R), and the intercept gives the natural log of the frequency factor.

The values for E_a and k' have been calculated by least squares, assuming a linear relation. Activation energies are 47 and 41 kcal/mol for Opx 4 and Opx 5, respectively, with associated frequency factors of 4.70×10^9 and 1.97×10^9. (R values are 88.6% for Opx 4; 99.9% for Opx 5.)

Activation energies as a function of composition are shown in Figure 8 and Table 4. The activation energies of the Mg-rich samples are approximately 60 kcal/mol. This includes sample M32B, for which the ordering activation energy, not the disordering activation energy, is calculated. The more Fe-rich samples have activation energies of approximately 45 kcal/mol. Again the ordering sample, PX4, shows an activation energy similar to those of the disordering samples. Sample 10 and sample TZ show significantly different activation energies for approximately the same composition. As results for sample

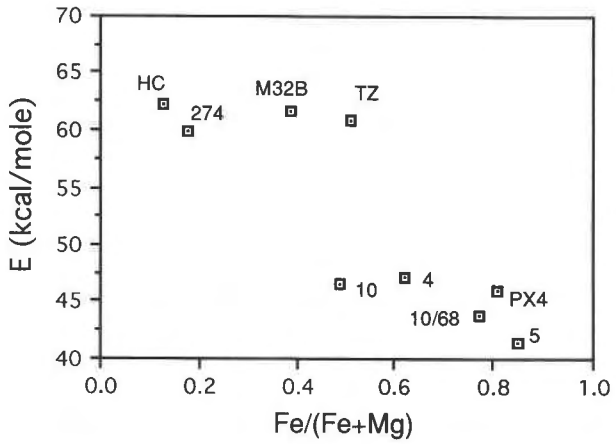

Fig. 8. Activation energies from Table 4 with respect to composition.

10 are only based on two measurements and sample TZ on four, the value for sample 10 may be in error, and further experimentation should be carried out on it.

Discussion

Reaction rate constants (calculated using the Mueller chemical rate law) show the expected increase with temperature and Fe^{2+} enrichment for all disordering studies. However, ordering studies give faster rates for disordered sample M32B and the same rate for PX4. Theoretically, ordering is expected to be a slower process than disordering, since there are more paths available for the system to disorder than to order (Putnis and McConnell, 1980). This indicates a possible problem with sample M32B or with the chemical rate law when it is applied to ordering.

Anovitz et al. (1988) disordered both samples by heating them at 900 °C for 2 h. As already stated, these conditions are outside the stability field of orthopyroxene for sample PX4. Although it is clearly shown by the experiments that both samples became progressively more ordered, the degree of order of the initial material is not fully known. The sample might have disordered further with time if held at 900 °C. O'Neill et al. (1991) have studied the variation in reaction rates for the cation distribution in magnesioferrite and found significant differences depending on the initial order of the sample relative to the equilibrium state. In addition, there may have been little long-range order but significant short-range order, which could speed up the ordering reaction (e.g., such as suspected in omphacites found in eclogites, Ross, 1991). Clearly, the chemical rate law as defined by Mueller does not account for reaction rate changes resulting from differences between the degree of order in the starting material and the degree of order at equilibrium.

A significant change in activation energy from the Mg-rich samples to the Fe-rich samples is shown by several site occupancy studies and two very different site defining techniques (Mössbauer and X-ray structure refinement). The Mg-rich samples have a higher activation energy of approximately 60 kcal/mol, and the Fe-rich samples have a lower activation energy of approximately 45 kcal/mol. The break is at approximately 50–60% Fs. This difference could be attributed to a change in the site exchange mechanism at approximately Fs_{50}–Fs_{60}. In this composition range the M2 site is almost saturated with Fe^{2+}, and Fe^{2+} must begin to enter the M1 site (Fig. 2). This affects the crystal structure, increasing the lengths of the M2-O3A and M2-O3B bonds (Fig. 3a and 3b; Domeneghetti et al., 1985). The opening up of the structure could make the exchange reaction faster. Several other factors could affect the activation energy, such as defect density or the types of defects. In addition, it is possible that at greater Fe^{2+} concentrations the amount of Fe^{3+} will be greater, causing an increase in vacancy concentration. This in turn increases the probability that a site will be available for exchange, i.e., the entropy is increased. All of these factors could account for a decrease in the activation energy for the compositional range Fs_{50}–Fs_{100}. A further, probably connected, feature has been found at this compositional range for macrocrystals. It is a break in slope of Fe^{2+}-Mg partitioning between Ca-rich and Ca-poor pyroxene, which was discussed by Huebner (1980, p. 227).

The Mueller chemical rate law yields consistent results for activation energy for both the ordering and disordering processes. As with Gibbs free energy, activation energy can be defined by the enthalpy and entropy of activation ($\Delta E_a = \Delta H_a - T\Delta S_a$). The entropy for disordering must be larger than the entropy for ordering. However, if the enthalpy is large relative to the entropy, very little difference would be seen between the activation energies of the two reactions.

Considering the above problems and the fact that the chemical rate law results are not easily incorporated into macroscopic thermodynamic functions, we suggest that a further study may be possible using Landau theory for nonconvergent ordering. Salje and Kroll (1990) have used reaction rate laws derived from order-parameter theory to describe the nonconvergent Al-Si order-disorder reaction in sanidine (only disordering experiments considered), and both the equilibrium values and the reaction rates are in good agreement with this theory.

Acknowledgments

We would like to thank reviewers James Besancon, Joseph Smyth, and Lawrence Anovitz for their comments, which significantly improved the contents of this paper. Also, thanks go to Michael Carpenter, Peter Heaney, Ekhard Salje, and Gordon Nord for their support and encouragement.

References cited

Anovitz, L.M., Essene, E.J., and Dunham, W.R. (1988) Order-disorder experiments on orthopyroxene: Implications for the orthopyroxene speedometer. American Mineralogist, 73, 1060–1073.

Besancon, J.R. (1981) Rate of cation disordering in orthopyroxenes. American Mineralogist, 66, 965–973.

Buseck, P.R., Nord, G.L., Jr., and Veblen, D.R. (1980) Subsolidus phenomena in pyroxenes. In Mineralogical Society of America Reviews in Mineralogy, 7, 117–212.

Chatterjee, N. (1987) Evaluation of thermochemical data on Fe-Mg ol-

ivine, orthopyroxene, spinel and Ca-Fe-Mg-Al garnet. Geochimica et Cosmochimica Acta, 51, 2515–2526.

Colby, J.W. (1972) MAGIC IV, a computer program for quantitative electron microprobe analysis. Bell Telephone Labs, Allentown, Pennsylvania.

Comer, D.T., and Waber, J.T. (1974) Atomic scattering factors for x-rays. In J.A. Ibers and W.A. Hamilton, Eds., International tables for X-ray crystallography, vol. IV, p. 71–103. Kynoch, Birmingham, U.K.

Cundari, A., and Salviulo, G. (1987) Clinopyroxenes from Somma-Vesuvius: Implications of crystal chemistry and site configuration parameters for studies of magma genesis. Journal of Petrology, 28, 727–736.

Davidson, P.M. (1985) Thermodynamic analysis of quadrilateral pyroxenes. I. Derivation of the ternary non-convergent site-disorder model. Contributions to Mineralogy and Petrology, 91, 383–389.

Davidson, P.M., and Lindsley, D.H. (1985) Thermodynamic analysis of quadrilateral pyroxenes. II. Model calibration from experiments and applications to geothermometry. Contributions to Mineralogy and Petrology, 91, 390–404.

Dienes, G.J. (1955) Kinetics of order-disorder transformations. Acta Metallurgica, 3, 549–557.

Domeneghetti, M.C., Molin, G.M., and Tazzoli, V. (1985) Crystal-chemical implications of the Mg^{2+}-Fe^{2+} distribution in orthopyroxenes. American Mineralogist, 70, 987–995.

Evans, B.J., Ghose, S., and Hafner, S. (1967) Hyperfine splitting of ^{57}Fe and Mg-Fe order-disorder in orthopyroxenes ($MgSiO_3$-$FeSiO_3$ solid solution). Journal of Geology, 75, 306–322.

Freeborn, W.P., McGee, E.S., and Huebner, J.S. (1985) MINCLC FORTRAN program for recalculating mineral analyses. U.S. Geological Survey Open-File Report 85-257.

Ganguly, J. (1982) Order-disorder in ferromagnesian silicates. II. Thermodynamics, kinetics and geological applications. Advances in physical geochemistry, 2, 58–100.

Ganguly, J., and Ghose, S. (1979) Aluminous orthopyroxene: Order-disorder, thermodynamic properties and petrological implications. Contributions to Mineralogy and Petrology, 69, 375–385.

Ghose, S. (1961) The crystal structure of a cummingtonite. Acta Crystallographica, 14, 622–627.

——— (1965) Fe^{2+}-Mg^{2+} order in an orthopyroxene. Zeitschrift für Kristallographie, 122, 81–99.

Huebner, J.S. (1980) Pyroxene phase equilibria at low pressure. In Mineralogical Society of America Reviews in Mineralogy, 7, 213–280.

James, F., and Roos, M. (1975) MINUIT, a system for function minimization and analysis of the parameter errors and correlations. Computer Physics Communications, 10, 343–367.

Khristoforov, K.K., Nikitina, L.P., Krizhanskiy, L.M., and Yekimov, S.P. (1974) Kinetics of disordering of distribution of Fe^{2+} in orthopyroxene structures. Døklady, Earth Science Section, 214, 165–168 (translated from Døklady Akademie Nauk SSSR, 214, 909–912, 1974).

Lindsley, D.H. (1983) Pyroxene thermometry. American Mineralogist, 68, 477–493.

Molin, G.M. (1989) Crystal-chemical study of cation disordering in Al-rich and Al-poor orthopyroxenes from spinel lherzolite xenoliths. American Mineralogist, 74, 593–598.

Molin, G.M., Saxena, S.K., and Brizi, E. (1991) Iron-magnesium order-disorder in an orthopyroxene crystal from Johnstown meteorite. Earth and Planetary Science Letters, 105, 260–265.

Mueller, R.F. (1962) Energetics of certain silicate solid solutions. Geochimica et Cosmochimica Acta, 26, 581–598.

——— (1967) Model for order-disorder kinetics in certain quasi-binary crystals of continuously variable composition. Journal of Physical Chemistry of Solids, 28, 2239–2243.

——— (1969) Kinetics and thermodynamics of intracrystalline distribution. Mineralogical Society of America Special Paper, 2, 83–93.

Nord, G.L., Jr., and McCallister, R.H. (1979) Kinetics and mechanism of decomposition in $Wo_{25}En_{31}Fs_{44}$ clinopyroxene. Geological Society of America Abstracts with Programs, 11, 488.

North, A.C.T., Phillips, D.C., and Mathews, F.S. (1968) A semi-empirical method of absorption correction. Acta Crystallographica, A24, 351–359.

O'Neill, H.St.C., Annersten, H., and Virgo, D. (1991) The temperature dependence of the cation distribution in magnesioferrite ($MgFe_2O_4$) from powder XRD structural refinements and Mössbauer spectroscopy. American Mineralogist, 77, 725–740.

Putnis, A., and McConnell, J.D.C. (1980) Principles of mineral behaviour, 257 p. Elsevier, New York.

Ross, C.R., II (1991) Ising models and geophysical applications. In J. Ganguly, Ed., Advances in physical geochemistry, vol. 8, p. 51–90. Springer-Verlag, Berlin.

Ross, M., and Huebner, J.S. (1975) A pyroxene geothermometer based on composition relationships of naturally occurring orthopyroxene, pigeonite and augite. International Conference on Geothermometry and Geobarometry, October 5–10, 1975, Extended Abstracts, Pennsylvania State University, University Park, Pennsylvania.

——— (1979) Temperature-composition relationships between naturally occurring augite, pigeonite, and orthopyroxene at one bar pressure. American Mineralogist, 64, 1133–1155.

Rossi, G., Smith, D.C., Ungaretti, L., and Domeneghetti, M.C. (1983) Crystal-chemistry and cation ordering in the system diopside-jadeite: A detailed study by crystal structure refinement. Contributions to Mineralogy and Petrology, 71, 257–269.

Salje, E.K.H., and Kroll, H. (1990) Kinetic rate laws derived from order parameter. III. Al, Si ordering in sanidine. Physics and Chemistry of Minerals, 17, 563–568.

Saxena, S.K. (1969) Distribution of elements in coexisting minerals and the problem of chemical disequilibrium in metamorphosed basic rocks. Contributions to Mineralogy and Petrology, 20, 177–197.

——— (1983a) Problems of two-pyroxene geothermometry. Earth and Planetary Science Letters, 65, 382–388.

——— (1983b) Exsolution and Fe^{2+}-Mg order-disorder in pyroxenes. Advances in Physical Geochemistry, 3, 61–80.

Saxena, S.K., and Ghose, S. (1971) Mg^{2+}-Fe^{2+} order-disorder and the thermodynamics of the orthopyroxene crystalline solution. American Mineralogist, 56, 532–539.

Saxena, S.K., Domeneghetti, M.C., Molin, G.M., and Tazzoli, V. (1989) X-ray diffraction study of Fe^{2+}-Mg order-disorder in orthopyroxene: Some kinetic results. Physics and Chemistry of Minerals, 16, 421–427.

Skogby, H., Annersten, H., Domeneghetti, M.C., Molin, G.M., and Tazzoli, V. (1992) Iron distribution in orthopyroxene: A comparison of Mössbauer spectroscopy and X-ray refinement results. European Journal of Mineralogy, 4, 441–452.

Smyth, J.R. (1973) An orthopyroxene structure up to 850°C. American Mineralogist, 58, 636–648.

Sposato, K.A., and Besancon, J.R. (1987) Determination of the 500°C equilibrium Fe-Mg site distribution isotherm in orthopyroxenes by Mössbauer spectroscopy. Geological Society of America Abstracts with Programs, 19, 853–854.

Sueno, S., Cameron, M., and Prewitt, C.T. (1976) Orthoferrosilite: High-temperature crystal chemistry. American Mineralogist, 61, 38–53.

Sykes, J.A. (1984) High-grade metamorphism of Fe^{2+}-rich bodies in Archean Gneiss, Wind River Mountains, Wyoming. M.S. thesis, University of Minnesota, Duluth, Minnesota.

Tazzoli, V., and Domeneghetti, M.C. (1987) Crystal-chemistry of natural and heated aluminious orthopyroxenes. Physics and Chemistry of Minerals, 15, 131–139.

Tokonami, M. (1965) Atomic scattering factor for O^{2-}. Acta Crystallographica, 19, 486.

Virgo, D., and Hafner, S.S. (1969) Order-disorder in heated orthopyroxenes. Mineralogical Society of America Special Paper, 2, 67–81.

——— (1970) Fe^{2+}-Mg order-disorder in natural orthopyroxenes. American Mineralogist, 55, 210–223.

Manuscript received August 29, 1991
Manuscript accepted May 3, 1993